New Journal of Physics
The open access journal at the forefront of physics

Deutsche Physikalische Gesellschaft DPG IOP Institute of Physics

PAPER • OPEN ACCESS

Ultra-fast two-qubit ion gate using sequences of resonant pulses

To cite this article: E Torrontegui *et al* 2020 *New J. Phys.* **22** 103024

New Journal of Physics
The open access journal at the forefront of physics

Deutsche Physikalische Gesellschaft DPG
IOP Institute of Physics

Published in partnership with: Deutsche Physikalische Gesellschaft and the Institute of Physics

OPEN ACCESS

RECEIVED
9 July 2020

REVISED
7 September 2020

ACCEPTED FOR PUBLICATION
22 September 2020

PUBLISHED
12 October 2020

PAPER

Ultra-fast two-qubit ion gate using sequences of resonant pulses

E Torrontegui[1,2], D Heinrich[3,4], M I Hussain[3,4], R Blatt[3,4] and J J García-Ripoll[1]

[1] Instituto de Física Fundamental IFF-CSIC, Calle Serrano 113b, 28006 Madrid, Spain
[2] Departamento de Física, Universidad Carlos III de Madrid, Avda. de la Universidad 30, 28911 Leganés (Madrid), Spain
[3] Institut für Quantenoptik und Quanteninformation, Österreichische Akademie der Wissenschaften, Technikerstr. 21a, 6020 Innsbruck, Austria
[4] Institut für Experimentalphysik, Universität Innsbruck, Technikerstr. 25, 6020 Innsbruck, Austria
* Author to whom any correspondence should be addressed.

E-mail: eriktorrontegui@gmail.com

Keywords: quantum information, trapped ions, qubit gates

Abstract

We propose a new protocol to implement ultra-fast two-qubit phase gates with trapped ions using spin-dependent kicks induced by resonant transitions. By only optimizing the allocation of the arrival times in a pulse train sequence the gate is implemented in times faster than the trapping oscillation period $T < 2\pi/\omega$. Such gates allow us to increase the number of gate operations that can be completed within the coherence time of the ion-qubits favoring the development of scalable quantum computers.

1. Introduction

Trapped ions are one of the most accurate platforms for scalable quantum computation. Many ions can be loaded in Paul traps [1, 2], Penning traps [3] or possibly in other scalable architectures [4, 5]. Within these traps, qubits can be stored in long-lived atomic states, which are individually manipulated using lasers or microwaves to implement high-fidelity single-qubit operations and measurements. Finally, using the vibrational states of the ion crystal mediators, it is possible to implement universal multiqubit operations, such as the CNOT gate [6, 7], the Mølmer–Sørensen gate [8, 9], geometric phase gates [10, 11] or Toffoli operations [12, 13]. The actual realization of many of these gates depends on Raman transitions [14–17], with high-fidelity [16, 17] and excellent coherence properties [18]. In practice, fidelity and speed of two-qubit gates are still limiting the depth of actual computations, and prevent the development of scalable fault tolerant computation [19].

Those limitations in fidelity and speed are due to the use of highly detuned lasers, with lengthy control procedures and slow dynamics of the vibrational states. There exist faster gates based on faster and stronger acceleration of the ions [20–23]. Already a strong time-dependent optical lattice may result in high-fidelity gates that are shorter than a trap period [24], but are still constrained by available detuning, power and the Lamb-Dicke limit [25]. Another method is to excite an optical transition using picosecond laser pulses. A properly designed pulse train can create an arbitrarily fast two- or multi-qubit gate [20, 21]. However, as demonstrated in reference [26], it remains a technical challenge to have a strong momentum kick per pulse—a Raman transition might not provide enough momentum—and to switch directions in the pulse laser—which may induce additional sources of error and decoherence.

In this work we study the realization of fast high-fidelity quantum gates using a train of laser pulses that excite a resonant transition [27]. We focus on a simple scenario that only requires pulse-picking from a train of laser pulses with fixed strength and repetition rate. As example, we study a realistic pulsed scheme driving the $4S_{1/2} \rightarrow 4P_{3/2}$ transition in $^{40}Ca^{+}$ [27]. We design the gate protocols with a two-stage global optimization that combines a continuous approximation with a discrete genetic algorithm for fine-tuning the pulse picking. We find many choices of pulses that implement highly entangling gates in a time

comparable to the trap frequency, with very weak sensitivity to the pulse arrival time or the temperature of the motional states.

The manuscript is structured as follows: in section 2.1, we revisit the theory for implementing phase gates using spin-dependent kicks [6, 20, 21]. Section 2.2 presents a possible experimental setup and an optimized control protocol based on state-of-the-art kicking and control of trapped ions [27]. The results leading to the implementation of ultra-fast two-qubit gates are discussed in section 3. In section 4 we analyze and quantify the main source of errors in the design of such gates. Finally, we present prospective research lines related to this work in section 5.

2. Methods

2.1. Geometric phase by state-dependent kicks

Consider two ions of mass m in a 1D-harmonic potential of frequency ω, at positions x_1 and x_2. Using the center-of-mass (c) and stretch-mode (s) coordinates, $x_c = (x_1 + x_2)/2$ and $x_s = x_2 - x_1$ the free Hamiltonian for this system reads $H_0 = \hbar\omega_c a_c^\dagger a_c + \hbar\omega_s a_s^\dagger a_s$. Here $\omega_c = \omega$ and $\omega_s = \omega\sqrt{3}$ and $a_{c,s}^\dagger$ ($a_{c,s}$) are the creation (annihilation) phonon operators for each mode. The ions interact with a laser beam that is resonant with an atomic transition. This interaction is modeled by the effective Hamiltonian

$$H_1 = \frac{\Omega(t)}{2}[\sigma_1^\dagger\ \mathrm{e}^{\mathrm{i}\hbar k x_1} + \sigma_2^\dagger\ \mathrm{e}^{\mathrm{i}\hbar k x_2} + \mathrm{H.c.}]. \tag{1}$$

The pseudospin ladder operator $\sigma_i^\dagger$ connects the ground and excited states of the ith ion—in this setup, the $4S_{1/2}$ and $4P_{3/2}$ states of $^{40}Ca^+$. The interaction accounts for processes where the ion absorbs or emits a photon, changing its internal state and also modifying its momentum by $\pm\hbar k$. The sign of k depends on the direction of the laser and whether the photon is emitted or absorbed. Without loss of generality, we will forego assuming that a single laser simultaneously addresses both ions with a common Rabi frequency $\Omega(t)$.

Our gate protocols [20] alternate free evolution $H = H_0$, where the laser is switched off ($\Omega = 0$), with a very fast, pulsed interaction kicking the ion. As shown in figure 1(b), we assume pairs of pulses coming from counter-propagating directions such the first pulse activates the selected transition and the second coherently de-excites the ion back to the lower energy configuration. The Rabi frequency $\Omega(t)$ and the duration of each pulse δt satisfy $\int_0^{\delta t}\Omega(\tau)\mathrm{d}\tau = \pi$ and $\delta t \ll 2\pi/\omega$. The pulses kick the ions, accelerating them along the same direction. In between each pair of kicks, the ions oscillate freely in the trap. The combination of both effects can be modeled analytically. The evolution operator for N pulses is $\mathcal{U} = \mathcal{U}_c\mathcal{U}_s$ with $\mathcal{U}_{c,s} = \prod_{n=1}^N U_{c,s}(t_n, z)$ and

$$\begin{aligned} U_c(t_n, z) &= \mathrm{e}^{\mathrm{i}\alpha_c(\sigma_1^z+\sigma_2^z)(a_c+a_c^\dagger)}\ \mathrm{e}^{\mathrm{i}\omega_c t_n a_c^\dagger a_c} \\ U_s(t_n, z) &= \mathrm{e}^{\mathrm{i}\alpha_s(\sigma_1^z-\sigma_2^z)(a_s+a_s^\dagger)}\ \mathrm{e}^{\mathrm{i}\omega_s t_n a_s^\dagger a_s}. \end{aligned} \tag{2}$$

The amplitudes $\alpha_c = \eta z/2^{3/2}$ and $\alpha_s = \alpha_c/3^{1/4}$ depend on the Lamb-Dicke parameter $\eta = \sqrt{\frac{\hbar}{2m\omega}}k$. The sign $z = \pm 1$ indicates the net orientation of the combined kick. It depends on the relative order of pulses within each pair: $z = +1$ if the first pulse comes from the left and the second from the right, $z = -1$ in the opposite case. In the setup from figure 1(b), the sign z is fixed to one of these values throughout the experiment.

A kicking sequence with N pulses displaces the Fock operators $a_{c,s}$ by a complex number $A_{c,s}$ that depends on the collective state of the ions

$$\begin{aligned} a_c \to\quad & a_c + A_c = a_c + \mathrm{i}(\sigma_1^z + \sigma_2^z)\alpha_c\sum_{n=1}^N \mathrm{e}^{-\mathrm{i}\omega_c t_n} \\ a_s \to\quad & a_s + A_s = a_s + \mathrm{i}(\sigma_1^z - \sigma_2^z)\alpha_s\sum_{n=1}^N \mathrm{e}^{-\mathrm{i}\omega_s t_n}. \end{aligned} \tag{3}$$

In phase space ($\langle x_{c,s}\rangle$, $\langle p_{c,s}\rangle$), the normal modes follow polygonal orbits (cf figure 2). The edges of the polygon all have uniform length $\sim\alpha_{c,s}$ and the angles between edges are determined by the arrival times of the kicks $\omega_c t_n$. A different frequency ω_c' rotates the same amount if the pulse is allocated at $t_n' = t_n\omega_c/\omega_c'$ leading to the same angle between consecutive edges. A perfect gate restores the motional state of the ion

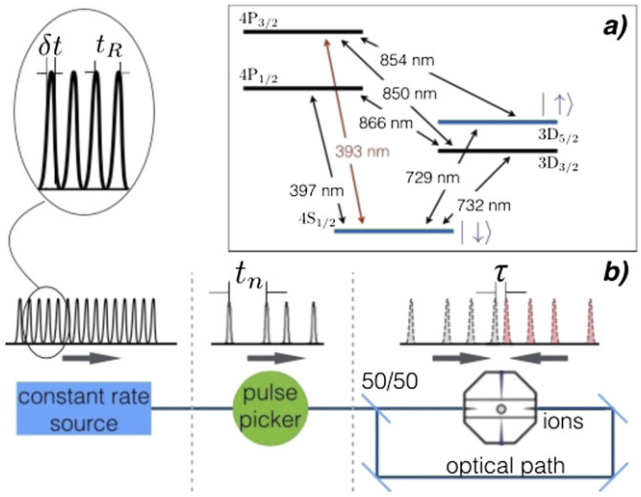

Figure 1. (a) Relevant levels of a $^{40}Ca^{+}$ ion. The qubit states $|\downarrow\rangle$ and $|\uparrow\rangle$ correspond to the $4S_{1/2}$ and $3D_{5/2}$ levels, respectively. A picosecond laser beam of 393.4 nm, resonant with the $4S_{1/2} \leftrightarrow 4P_{3/2}$ transition, imparts spin-dependent kicks to the ion. (b) (Bottom) Experimental setup. A constant rate source generator creates pulses with an interval t_R. A pulse picker selects the t_n optimal positions and a 50/50 beamsplitter divides each pulse. Both sequences follow a different optical path such that when they arrive at the ion in counter-propagating directions each left-right pulse pair has a relative delay τ much shorter than the characteristic decay time of the selected transition t_γ. (Top) Pulse train at each stage of the experiment, the black arrows represent the motional sense of the pulses.

$A_c = A_s = 0$, bringing them back to their original oscillator trajectories

$$\sum_{n=1}^{N} e^{i\omega t_n} = \sum_{n=1}^{N} e^{i\sqrt{3}\omega t_n} = 0, \tag{4}$$

and closing the orbits. Under these conditions, after a time T the evolution operator becomes [20]

$$\mathcal{U}(\phi, T) = e^{-i\phi\sigma_1^z\sigma_2^z}\ e^{i\omega_c T a_c^\dagger a_c}\ e^{i\omega_s T a_s^\dagger a_s}. \tag{5}$$

This is equivalent to free evolution in the trap, combined with a global phase ϕ that does not depend on the motional state,

$$\begin{aligned}\phi &= \alpha_c^2 \sum_{j=2}^{N}\sum_{k=1}^{j-1}\left[\frac{\sin(\sqrt{3}\omega(t_j - t_k))}{\sqrt{3}} - \sin(\omega(t_j - t_k))\right] \\ &=: \alpha_c^2\varphi.\end{aligned} \tag{6}$$

When equation (4) holds and the total phase satisfies

$$\phi = \pi/4 + 2n\pi \quad n \in \mathbb{Z}, \tag{7}$$

the combined evolution implements a control-phase gate on the internal state of the ions. The set of equations that determines the operation of the gate are solved in two steps. First, calculating the allocation positions $x_n = \omega t_n$ that fulfill equation (4) and determines the value φ, see equation (6). The determination of x_n leads to equivalent different pulse sequences where the new pulse arrival times are re-scaled $t'_n = t_n\omega/\omega'$ but the value of φ holds. Second, we change the trapping frequency and scale the arrival times to calibrate the Lamb-Dicke parameter and the amplitude α_c, to implement a control-phase gate (7). The new trapping frequencies are given by

$$\omega = \frac{\hbar k^2 \varphi}{16m(\pi/4 + 2n\pi)}. \tag{8}$$

Given an optimal pulse sequence and closed phase-space trajectory (4), there are several trapping frequencies (8) that implement the same gate. These frequencies are found to overshoot the accumulated phase, exceeding the minimum value $\pi/4$ by an integer multiple n of 2π. As we will see later, a clever choice of overshoot factors n allows us to fine tune the frequency within experimentally reasonable bounds.

The control scheme presented above relies on the interaction Hamiltonian (1), characteristic in trapped ions setups. Such interaction is independent of the considered species. However, the selected resonant

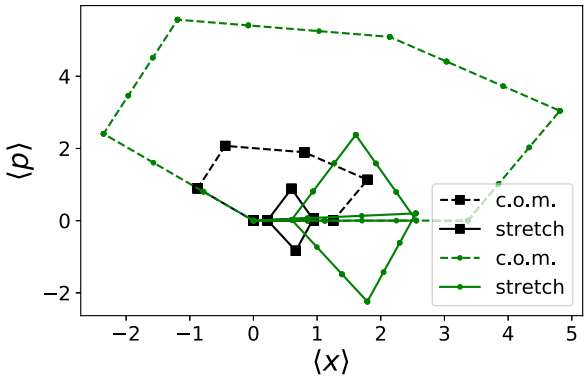

Figure 2. Phase space trajectories for the center-of-mass (dashed) and stretch mode (solid) for a pulse sequence with $N = 6$ sets of pulses, with $M = 1$ pulses (black) and $M = 3$ pulses (green) per set, respectively. The trajectories are drawn in the frame of reference that rotates with the frequency of the mode, that is $\langle a e^{i\omega_{c,s}t}\rangle = \frac{1}{\sqrt{2}}\langle x_{c,s}\rangle + \frac{i}{\sqrt{2}}\langle p_{c,s}\rangle$ for the center-of-mass (c) and stretch (s) mode.

transition must be able to displace the ions and accumulate a phase. As the displacements in phase space are proportional to the wavenumber k the scheme is suitable for optical transitions, but less energetic transitions such microwave controls do not provide enough momentum to the ion to accumulate the requested phase.

2.2. Experimental setup and parameters

We propose to implement the ultra-fast two-qubit gate using $^{40}Ca^{+}$ ions confined in a Paul trap with center-of-mass frequency $\omega \in [\omega_{\min}, \omega_{\max}]$. The relevant internal levels of the ion are depicted in figure 1(a). The qubit is stored in the $4S_{1/2}$ and $3D_{5/2}$ states and we use the $4S_{1/2} \leftrightarrow 4P_{3/2}$ transition to kick the ion.

As shown in figure 1(b), a single source generator produces a continuous train of pulses. A pulse picker selects pulses with discrete arrival times t_n compatible with a gate protocol. The discreteness of the arrival times transforms our gate design into a combinatorial optimization problem, described in section 2.3. Each pulse is split into two identical components by a 50/50 beam splitter. The two pulses arrive at the ion with a relative delay τ, controlled by the relative length of the two optical paths. The ion is excited by the first pulse, which in figure 1(b) comes from the left. By absorbing a photon, the ion acquires a momentum $+\hbar k$. Shortly after this, a second pulse coming from the counter-propagating direction (right in figure 1(b)) deexcites the atom. The act of emitting a photon in the opposite direction, with momentum $-\hbar k$, increases the momentum of the ion by $+\hbar k$. The combined action of both pulses amounts to a very fast kick with momentum $+2\hbar k$.

To implement our phase gate, we assume a pulsed laser with these characteristics: (i) the laser is resonant with the ion transition, operating at a central frequency of 393.4 nm. (ii) The repetition rate of the laser $R \sim 5$ GHz is much faster than the experimentally motivated trap frequencies $\omega \in 2\pi \times [78\text{ kHz}, 2\text{ MHz}]$, allowing a fine-grained control of the pulse sequences. (iii) The length of the pulses δt and the delay between kicks τ are both shorter than the lifetime of the $4P_{3/2}$ state, $\delta t, \tau \ll t_\gamma = 6.9$ ns. This allows us to neglect spontaneous emission during the pulsed excitation and during the dark times. (iv) The area of the pulses is calibrated to fully transfer all probability between the $4S_{1/2}$ and $4P_{3/2}$ states, i.e. $\int_0^{\delta t} \Omega(\tau)\mathrm{d}\tau = \pi$. Almost all requirements, except for the splitting and delay of pulses, have been demonstrated by frequency-quadrupling the light generated by a commercial laser [27].

2.3. Design and optimization of a discrete control

Section 2.1 established that a control-phase gate can be implemented by a sequence of pulse pairs that satisfies equations (4) and (7). In this work we address the design of the pulse sequence as two consecutive tasks: (i) find a set of pulse arrival times $\{t_n\}_{n=1}^{N}$ that meet conditions (4), (ii) fine tune the trapping frequency ω so that the total acquired phase is compatible with the implementation of a control-phase gate (7).

The first task decides our pulse picking strategy. To measure the goodness of the sequences fulfilling (4) we define the gate error ϵ that accounts for the ability to restore the motional state of the ions. Note that the total Hamiltonian $H = H_0 + H_I$ is quadratic in the phonon operators for both the c- and s-modes. Therefore, a Gaussian state remains Gaussian after the whole kicking sequence. The lack of overlap between the initial state located at the origin $(0, 0)$ and the final state produced by the pulse sequence located at

$(|A_c|, |A_s|)$ defines ϵ which in the small displacement limit, i.e. $|A_c|, |A_s| \to 0$, takes the form

$$\epsilon = |A_c|^2 + |A_s|^2, \tag{9}$$

that implicitly depends on the amount of applied pulses.

The minimization of ϵ implies solving a combinatorial optimization problem, where the times $t_n = k_n \times t_R + t_1$ are spaced by integer multiples of the laser pulse period t_R. In phase space, equation (4) ensures closed polygonal trajectories (cf figure 2), with angles between edges proportional to $\omega_{c,s}(t_{n+1} - t_n)$ and edge lengths proportional to $\alpha_{c,s}$. The area enclosed by the polygons determines the geometric phase ϕ. By adjusting the trap frequency ω_c, we tune the kick strengths $\alpha_c = \alpha_c(\omega)$, scaling the whole trajectory in phase space. This allows us to fine tune the accumulated phase (7) to the desired value, modulo an irrelevant integer n.

The design of the pulse sequence is a hard combinatorial optimization problem, where we pick N pulses out of a much longer train. To avoid the exponential complexity in this search, we find good approximate solutions using a two-stage method. The first stage is a regular minimization of the gate error ϵ over a set of N continuous arrival times $t_n \in \mathbb{R}$. We apply a standard algorithm to minimize the gate error (9) over a set of N variables, using K_{seed} random initial seeds $\vec{t} \equiv \{t_1, t_2, \ldots, t_N\}$ of ordered times $t_{n+1} > t_n$ and $t_N \leqslant 2\pi/\omega$. We select a subset of K_{opt} controls maximizing the phase ϕ, rejecting slow solutions $T > 2 \times 2\pi/\omega$. In the second stage of this process, we introduce the finite repetition of the laser. We round the K_{opt} continuous solutions to the nearest laser pulses, which are spaced by a multiple of $t_R = 1/R$. These discrete protocols introduce a possible timing error $\xi = |t_n - nt_R|$. Instead of just a local minimization of each ξ, we minimize the global error (9) with a genetic algorithm that fine tunes the pulse allocation.

A genetic algorithm [28, 29] is a discrete optimizer that builds on the concept of natural selection, where solutions are iteratively improved using biologically inspired operations such as selection, crossover and mutation. In each iteration, a set or *population* is composed by several candidate solutions (called *individuals*) and are evolved towards better solutions based on a *fitness* function—the cost function to be optimized. On each iteration or *generation*, the algorithm selects a subset of individuals that maximize the fitness. These so called *parents* merge and mutate, giving rise to new solutions, the *offspring* that form the next generation. This process of selection and reproduction is repeated until the fitness reaches the desired optimal value, selected by a user-defined tolerance, or until the maximum number of generations is reached.

To bring our problem into this form, we take the N continuous times t_n and find out the M_{max} closest pulses within the discrete sequence created by the laser (cf figure 3(a)). We then encode a solution as a *chromosome* with $N \times M_{max}$ *genes*. Each gene is a bit that becomes 1 when the corresponding pulse is selected or 0 otherwise (cf figure 3(b)). Taking the optimal solution provided by the regular minimization we generate a seed. Our initial population is formed by K_{ind} individuals that results from rounding to nearest and randomly distributing M active genes within the M_{max} discrete positions at each $\{t_n\}_{n=1}^{N}$. As result each individual has $N \times M$ active genes, indicating that we have N groups of M pulses around the times t_n. From this pool, we select a subset of K_p parents as the individuals exhibiting the best value of the fitness function (9). Parents mate in pairs and each offspring receives part of its chromosome from the first parent and the rest from the second. In our algorithm this proportion is 50/50 made at the middle of each parent chromosome, see figure 3(b). If an offspring improves the fitness function it joins the parents to constitute the new population for the next generation. If not, a mutation is produced on the offspring creating random variations in the chromosome. To preserve the total number of $N \times M$ pulses, we randomly swap the values of two genes from a M_{max} sequence placed around one of the times t_n, see figure 3(b). These mutants join the new population, irrespective of their value of the fitness function, and the whole process is repeated. This workflow, sketched in figure 3, is repeated over K_{ite} generations. At the end, we select the individual that produces the best value of the fitness function, thereby minimizing the error equation (9).

For the two-stage optimization strategy the regular minimization of equation (9) represents the main computational cost that grows with N as the number of unknown variables t_n to be optimized becomes larger. Once the solutions fulfilling the commensurability equation (4) are obtained and fed into the genetic algorithm, the discrete minimization in contrast does not involve significant computational resources. The optimizer only needs to evaluate equation (9) for different sequences that are obtained by replacing part of the genes $0 \leftrightarrow 1$ using the crossover and mutation processes explained above. Based on the randomness in the generation of new solutions, for our simulations, the algorithm needs a computational time $\mathcal{O}(\text{secs})$ to provide a minimization improvement of the gate error ϵ that range from 0, where the initial seed corresponding to a local minimization of ξ represents the optimal solution, to cases where the genetic algorithm improves 2–3 orders of magnitudes the solution.

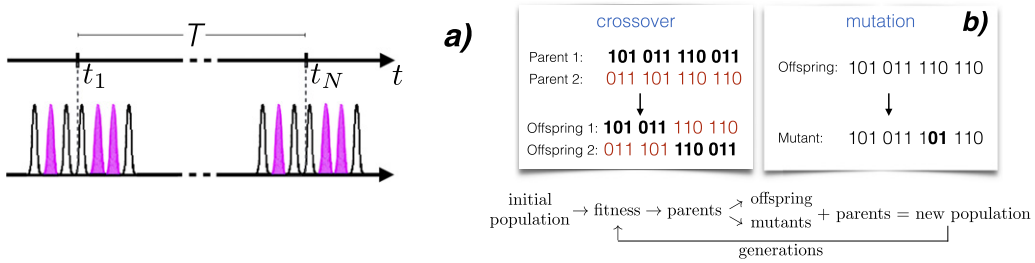

Figure 3. (a) Pulses from the equispaced sequence provided by a constant rate generator (bottom) are allocated in N discrete positions to approximate the optimal continuous delay times t_n (top). Concatenating M pulses around each optimal t_n position increases the gate's phase ϕ, keeping the same implementation time T. The genetic algorithm performs the optimization over $M_{\max}$ pulses around t_n and selects the M pulses that minimize the gate error ϵ, see equation (9). In the figure $M = 3$ (light shadows), and $M_{\max} = 7$. (b) Top: Crossover and mutation operations. In this example $N = 4$, $M = 2$, and $M_{\max} = 3$. Bottom: Genetic algorithm workflow.

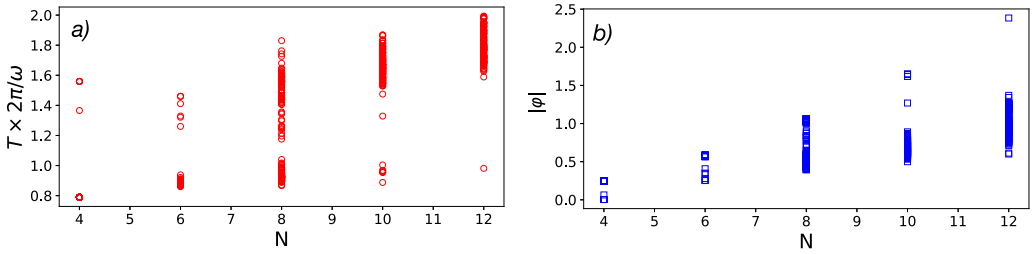

Figure 4. Partial gate optimization assuming full control over pulse arrival times. (a) Duration of pulse sequences satisfying equation (4) as a function of the number of applied pulses N. (b) Corresponding phase as a function of N.

3. Results

As mentioned above, our simulations consider a scenario where the direction of the kicks is fixed. This happens when a single pulse picker is connected to an interferometric setup, creating pairs of pulses all arriving with the same relative delay [cf figure 1]—e.g. the left pulse always excites the ion and the right pulse immediately de-excites it, setting $z = +1$. Scenarios where both the relative direction and the Lamb-Dicke parameter are tuned have been considered before [20, 22, 30, 31] leading to different degrees of controllability and thus to different gate times. Here we will show that, despite our experimentally-motivated constraints [27], it is possible to implement control-phase gates in a time shorter than the trap period $T < 2\pi/\omega$.

Before illustrating the final protocols, figure 4 shows the intermediate results obtained when solving the commensurability equation (4) with continuous variables $\{t_n\}_{n=1}^{N}$. Note how for a fixed number of pulses N there exist multiple schemes that restore the motional state of the ions and implement a control-phase gate. Out of those combinations we select those that maximize the ratio $\varphi = |\phi/\alpha_c^2|$, and feed them to the genetic algorithm to create discrete pulse sequences. Note that the two-qubit phase depends on α_c and therefore on the trap frequency ω_c. The preselection of continuous protocols with large φ provides a broader choice of pulse sequences and frequencies (8) that satisfy both the experimental restriction $\omega \in [\omega_{\min}, \omega_{\max}]$ and the phase relation equation (7), with either $n = 0$ or $n \neq 0$ (*overshooting*).

A numerical fit shows that for the sequences maximizing the accumulated phase, phase grows with the number of pulses in the discrete protocol as $|\varphi| \propto N^{0.6}$, (cf figure 5(a)), while the duration of the gate remains below $T \lesssim 1.055 \times 2\pi/\omega$ and is close to the sequences minimizing the gate time T [cf figures 4(a), 5(b), and 7(a)]. When solving equation (4) for x_n this fit avoids the re-scaling of the arrival times t_n since it allows to fine tune in advance the frequency (8) leading to a control-phase gate as φ is known. The error introduced by the finite repetition rate is also negligible, figure 5(c) shows the theoretical error for one protocol consisting of $N = 6$ pulses. The global optimization of ϵ performed with the genetic algorithm (blue-solid) provides pulses sequences that minimize the gate error several orders of magnitude compared to the local minimization of ξ that rounds the continuous solutions allocating the pulses to the nearest discrete time nt_R compatible with the source repetition rate (red-dashed). A laser with a repetition rate $R \gtrsim 1$ GHz already produces an ultra-fast two-qubit gate with fidelity above 99.999%.

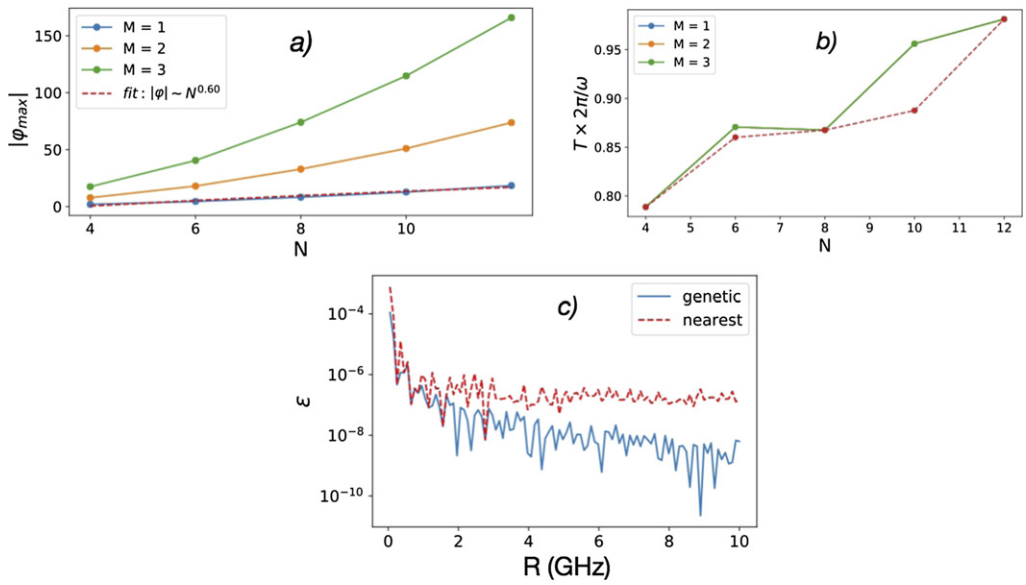

Figure 5. Optimal gates for discrete pulse arrival times. (a) Phase vs. number of batches N and number of pulses per batch M, for $R = 5000\omega$. When $M = 1$, maximum phase (blue solid line) grows as $|\varphi| \sim N^{0.6}$ (red-dashed line). Clustering $M = 1, 2, 3$ (blue, orange, green) of pulses around the optimal t_n times allow us to increase the phase. (b) The total gate duration is insensitive to the number of pulses per batch, and approaches the shortest gate for continuously varying pulse arrival times (dashed red). (c) Error (9) of the phase gate ($N = 6, M = 1$) as a function of the repetition rate R for a local minimization of $\xi = |t_n - nt_R|$ (red-dashed) and a global minimization using a genetic algorithm (blue-solid).

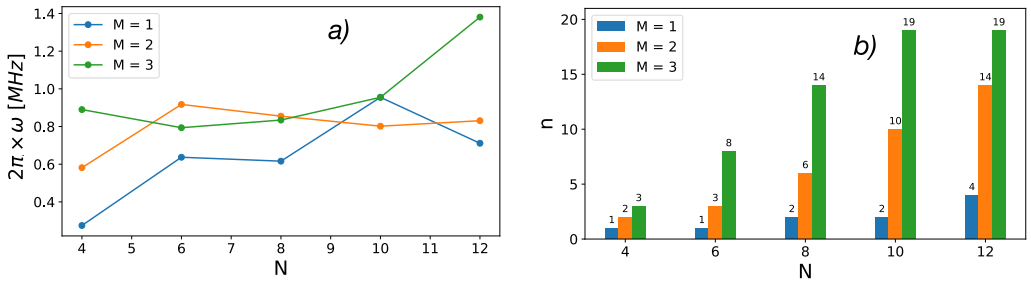

Figure 6. (a) Trapping frequencies associated with each phase gate depicted in figure 5. The frequencies are tuned such the frequency fulfilling (7) is closest to the reference trapping frequency $\omega = 2\pi \times 0.82$ MHz [27] selected as example. (b) Overshoot value of the phase $\phi = \pi/4$ associated with the trapping frequencies showed in (b) when implementing the gate.

As shown in figure 5(b), a short sequence with $N = 4$ pulses produces very fast gates $T < 2\pi/\omega$, but with a small acquired phase. We may increase the accumulated φ, concentrating M pulses around each of the N kicking times [cf figure 3(a)]. This maintains the shape of the orbits, scaling the edges by a factor of M [cf figure 5(a)]. As shown in figures 5(a) and (b), the duration of the gate is preserved and the accumulated phase grows with the area as $\varphi \propto M^2$. Note that, since the phase increases in discrete steps, we still need to fine tune the trap frequency to match the desired control-phase gate. Figures 6(a) and (b) show that this is possible for realistic trapping frequencies [27], using different multiplication factors M. Due to the existence of multiple compatible frequencies in the range $\omega \in 2\pi \times [78\,\text{kHz}, 2\,\text{MHz}]$ depending on the overshooting factor n, in figure 6(a) we show the frequencies (8) that implement a control-phase gate and which are closest to a specific reference frequency $\omega \sim 2\pi \times 0.82$ MHz [27] chosen as an example. As φ grows with both N and M, figure 6(b) shows that the specific frequency is achievable compensating the phase with a large overshooting factor n.

This resonant pulse scheme is intrinsically limited to kicks along the same direction. In the rotating reference frame, two consecutive segments (kicks) are separated an angle that depends on the waiting time and the direction of the kicks. In our scheme, the angle always grows in the same direction, due to kicks having the same orientation. Consequently, both the c- and s-modes describe closed polyhedral orbits—with edges that have the same length—only when the pulse sequence takes about a trap period, $T \sim 2\pi/\omega = T_\omega$, see equation (4). If we preserve this approximate duration for sequences with large number of pulses N, then angles decrease and the asymptotic orbits ($N \gg 1$) approximate distorted ellipses

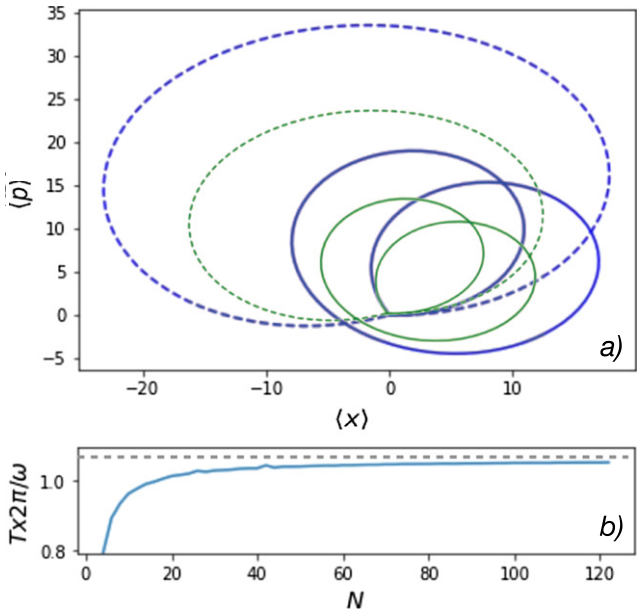

Figure 7. (a) Phase space trajectories for the center-of-mass (dashed) and stretch mode (solid) in the large N asymptotic limit, $N = 80$ (green) and $N = 120$ (blue) for the fastest gate within the sequence. (b) Fastest gate time T as a function of the applied pulses N. These sequences asymptotically fulfills $T \lesssim 1.055 \times 2\pi/\omega$ (dashed line).

that have similar shapes, but grow in area with N, see figure 7. As we showed, sequences with small numbers of pulses can improve over this asymptotic behavior, producing gates in shorter times $T < T_\omega$, independently of the concatenated amount of M pulses around t_n.

We could even improve further if we can control the magnitude of the acceleration of each kick, or the orientation. For example, if we can switch the order in which the pulses arrive, the momentum kick can take different signs ± 1 at each kick time, producing sequences where the gate time decreases with the number of pulses N. In this context, the angles are free to evolve and gates $T \ll T_\omega$ are feasible. Additionally, if we provide even more controllability, for example tilting the laser with respect to the axial trapping axis [20] leads to even faster gates. This extra-controllability is still an experimental challenge and may induce other sources of error.

4. Estimation of errors

We have presented a route for the implementation of ultra-fast $T < 2\pi/\omega$ quantum gates using a train of laser pulses that are resonant with the transition frequency of a trapped ion. In these protocols, the motional state of the ion is almost perfectly restored with a high-fidelity $\epsilon \sim 10^{-9}$–10^{-7} using source generators with a constant repetition rate $R \sim 5$ GHz. When implementing these protocols, actual experiments will suffer from imperfections in the control of the ion, due to spontaneous emission during the time that the ion remains in the excited state $4P_{3/2}$ (i.e., during pulses and waiting time), and due to intensity fluctuations in the pulses.

A trivial model to quantify the spontaneous emission errors, giving an upper bound on them, is to write a density matrix

$$\rho = (1 - P_{\rm err})|\psi\rangle\langle\psi| + P_{\rm err}|g\rangle\langle g| \tag{10}$$

where $|g\rangle$ is a fictitious state accumulating the probability that an error took place. The fidelity is given by $P_{\rm err}F_0$, where F_0 is the fidelity of the gate implemented by ideal kicks. In this model, $P_{\rm err}$ feeds from spontaneous emission effects: we assume that whenever the emission takes place, the experiment must be repeated. The probability that the ion is in an excited state $|e\rangle$ is

$$\frac{{\rm d}P_{\rm ok}}{{\rm d}t} = -\gamma|\langle e|\psi(t)\rangle|^2(1 - P_{\rm err}), \tag{11}$$

with $P_{\rm ok}+P_{\rm err}=1$. The decay rate $\gamma=1/t_\gamma$ is inversely proportional to the lifetime t_γ. The solution to this problem is

$$\begin{aligned}\epsilon_\gamma &= 1-P_{\rm ok}(T),\\ P_{\rm ok}(T) &= \exp\left(-\gamma\int_0^T |\langle e|\psi(t)\rangle|^2 {\rm d}t\right) P_{\rm ok}(0).\end{aligned} \tag{12}$$

In a very crude scenario, we upper bound the error probability, assuming that the ion is in the excited state from the beginning of the exciting pulse, to the end of the following, that is $T_{\rm e}\simeq \delta t+\tau$,

$$\epsilon_\gamma = 1-\exp(-\gamma T_{\rm e})\simeq \gamma T_{\rm e}. \tag{13}$$

In the experimental setup from figure 1(b), the waiting time τ between counter-propagating pulses is controlled by the relative length of the optical paths. The minimum separation is given by the pulse duration, $\tau\gtrsim\delta t$ to avoid interference. In our system, the excited state $4{\rm P}_{3/2}$ has a lifetime $t_\gamma=6.9$ ns and $T_{\rm e}\simeq 1$ ps [27, 32] leading to errors $\epsilon_\gamma\sim\mathcal{O}(\delta t/t_\gamma)\simeq 1.4\times10^{-4}$. For a sequence containing N kicks, the infidelity of the gate is approximately $\epsilon_\gamma^{\rm gate}=1-(1-\epsilon_\gamma)^N\sim\mathcal{O}(N\delta t/t_\gamma)$.

We can also quantify the errors $\epsilon_{\rm A}$ due to fluctuations in the $\pi-$pulses. For a general pulse shape $\theta=\int_0^{\delta t}\Omega(\tau){\rm d}\tau$ the unitary generated by the interaction Hamiltonian (1) is

$$\hat{U}_k=\left(c-{\rm i}s\hat{\sigma}_1^x\ {\rm e}^{{\rm i}kx_1\hat{\sigma}_1^z}\right)\left(c-{\rm i}s\hat{\sigma}_2^x\ {\rm e}^{{\rm i}kx_2\hat{\sigma}_2^z}\right) \tag{14}$$

with $c=\cos(\theta/2)$ and $s=\ \sin(\theta/2)$. A perfect $\pi-$pulse, i.e. $\theta=\pi$, generates the unitary $\hat{U}_{\rm kick}=-\hat{\sigma}_1^x\hat{\sigma}_2^x\ {\rm e}^{{\rm i}k(x_1\hat{\sigma}_1^z+x_2\hat{\sigma}_2^2)}$. In order to quantify the errors due to area fluctuations when combining two counter-propagating pulses $\hat{U}_{\rm pair}=\hat{U}_k\hat{U}_{-k}$ we consider small fluctuations $\pi+\Delta\theta=\int_0^{\delta t}\Omega(\tau){\rm d}\tau$ (with $\Delta\theta\to0$) in the pulse area. Retaining the first order terms in $\Delta\theta$ an imperfect pair of counter-propagating pulses generates the transformation

$$\hat{U}_{\rm pair}=(1-\Delta\theta^2/2)\hat{U}_0-\Delta\theta\hat{U}_e^1-\Delta\theta^2\hat{U}_e^2+\mathcal{O}(\Delta\theta^3) \tag{15}$$

with $\hat{U}_0={\rm e}^{-2{\rm i}k(x_1\hat{\sigma}_1^z+x_2\hat{\sigma}_2^z)}$ the optimal unitary generated by two perfect counter-propagating $\hat{U}_{\rm kick}$ pulses, and $\hat{U}_e^1={\rm i}(\sigma_1^x\ \cos(kx_1){\rm e}^{-2{\rm i}k\hat{\sigma}_2^zx_2}+\sigma_2^x\ \cos(kx_2){\rm e}^{-2{\rm i}k\hat{\sigma}_2^zx_1})$ and $\hat{U}_e^2=\cos(kx_1)\cos(kx_2)\hat{\sigma}_1^x\hat{\sigma}_2^x+({\rm e}^{{\rm i}kx_1\hat{\sigma}_1^z}+{\rm e}^{{\rm i}kx_2\hat{\sigma}_2^z})/4$ accounting for unrestored and incorrect motional dynamics. The total unitary of a gate can be approximated by the product of N pairs

$$\hat{U}_{\rm gate}\approx(1-\Delta\theta^2N/2)\hat{U}_N-N\Delta\theta\hat{U}_{\rm err} \tag{16}$$

with $\hat{U}_N=\hat{U}_0^N$ and collecting all the errant dynamics in $\hat{U}_{\rm err}$ that it is assumed orthogonal to the ideal unitary $\hat{U}_0$. This is a conservative approximation that neglects terms that result in an incorrect motional state, but includes those that correctly restore the internal state [31]. For any initial state $|\psi\rangle$ of the computational basis we can compare the dynamics of the optimal gate $\hat{U}_{\rm opt}$ with the one generated by $\hat{U}_{\rm gate}$. To this end we estimate the fidelity

$$F=|\langle\psi|\hat{U}_{\rm opt}^\dagger\hat{U}_{\rm gate}|\psi\rangle|^2=(1-N\epsilon_{\rm A}+N^2\epsilon_{\rm A}^2/4)F_0, \tag{17}$$

with $\epsilon_{\rm A}=\Delta\theta^2$. The magnitude of the fluctuations $\epsilon_{\rm A}$ depends on the specific characteristics of the laser pulses. In real setups with picosecond pulses [27, 33] these fluctuations are found to induce errors of around $\epsilon_{\rm A}\propto\Delta I/I\sim10^{-3}$. However, these intensity fluctuations can be reduced experimentally, using methods such as adiabatic rapid passages with chirped laser pulses [34–36].

5. Outlook

Our analysis shows that it is possible to engineer ultra-fast gates $T<2\pi/\omega$, using pulse picking strategies for an experimentally relevant setup [27, 32]. Current two-qubit Mølmer–Sørensen gate operations require a duration of $\bar{T}\sim40\ \mu$s for entangling two qubits at a trapping frequency $\omega\simeq2\pi\times1.4$ MHz [19]. Compared to these numbers, our scheme can provide a speedup factor $\bar{T}/T>50$, for a conservative gate duration $T\sim2\pi/\omega$.

Our investigation leaves some open questions, to be addressed in later works. The first one concerns the robustness of the protocol with respect to intensity fluctuations and spontaneous emission. Both problems may be overcome if we use STIRAP techniques [37–39], to induce excitation between the $4S_{1/2}$ and a metastable state, such as $3D_{5/2}$ or $3D_{3/2}$. Experimentally, $^{40}Ca^{+}$ ions have been robustly manipulated using such techniques [40–42]. For our proposal, we could detune the pulsed laser exciting the $4S_{1/2} \rightarrow 4P_{3/2}$ transition and combine it with another pulse connecting the $4P_{3/2} \leftrightarrow 3D_{5/2}$ states. These improvements can be supplemented with pulse shaping techniques [43–45], to minimize the AC Stark-shifts and dephasing associated with high-intensity pulses.

A second, more pressing question, concerns the parallelizability and scalability of our pulsed schemes. Recent works have addressed theoretically [21, 46, 47] and demonstrated experimentally [48, 49] the simultaneous implementation of arbitrary two-qubit gates among a subset or all pairs of K ions in a trap. We can use our two-step protocol to perform this task with significant speed ups. As in this work, the first step is a continuous optimization of the desired gate operation, subject to the now $2K$ dynamical constraints [21]. The resulting pulsed protocol is fine tuned with our genetic algorithm, to match the repetition rate of the laser. The process has an increased optimization cost, but the multi-qubit gates do not seem to take longer than the two-qubit ones [21].

Current ion trap quantum computers are able to run programs with up to several hundred one and two-qubit operations [50]. We expect that these methods and subsequent improvements ion trap quantum computers will be able to improve at least one, if not two orders of magnitude, leading to an increased quantum volume in NISQ devices. Moreover, the estimated ideal gate fidelities are compatible with existing error thresholds [51], which makes these methods a promising alternative for implementing fault-tolerant computation schemes [19].

Acknowledgments

We acknowledge support from Project PGC2018-094792-B-I00 (MCIU/AEI/FEDER,UE), CSIC Research Platform PTI-001, and CAM/FEDER Project No. S2018/TCS-4342 (QUITEMAD-CM). Authors also acknowledge support by the Institut für Quanteninformation GmbH.

References

[1] Porras D and Cirac J I 2004 *Phys. Rev. Lett.* **92** 207901
[2] Zhang J, Pagano G, Hess P W, Kyprianidis A, Becker P, Kaplan H, Gorshkov A V, Gong Z-X and Monroe C 2017 *Nature* **551** 601–4
[3] Jordan E, Gilmore K A, Shankar A, Safavi-Naini A, Bohnet J G, Holland M J and Bollinger J J 2019 *Phys. Rev. Lett.* **122** 053603
[4] Lekitsch B, Weidt S, Fowler A G, Mølmer K, Devitt S J, Wunderlich C and Hensinger W K 2017 *Sci. Adv.* **3** e1601540
[5] Jain S, Alonso J, Grau M and Home J P 2018 arXiv:1812.06755
[6] Cirac J I and Zoller P 1995 *Phys. Rev. Lett.* **74** 4091–4
[7] Schmidt-Kaler F *et al* 2003 *Nature* **422** 408–11
[8] Sørensen A and Mølmer K 1999 *Phys. Rev. Lett.* **82** 1971–4
[9] Sackett C A *et al* 2000 *Nature* **404** 256–9
[10] Milburn G J, Schneider S and James D F V 2000 *Fortschr. Phys.* **48** 801–10
[11] Leibfried D *et al* 2003 *Nature* **422** 412–5
[12] Toffoli T 1980 *International Colloquium on Automata, Languages, and Programming* pp 632–44
[13] Monz T, Kim K, Hänsel W, Riebe M, Villar A S, Schindler P, Chwalla M, Hennrich M and Blatt R 2009 *Phys. Rev. Lett.* **102** 040501
[14] Wolf F, Wan Y, Heip J C, Gebert F, Shi C and Schmidt P O 2016 *Nature* **530** 457–60
[15] Kaufmann H, Ruster T, Schmiegelow C T, Luda M A, Kaushal V, Schulz J, von Lindenfels D, Schmidt-Kaler F and Poschinger U G 2017 *Phys. Rev. Lett.* **119** 150503
[16] Ballance C J, Harty T P, Linke N M, Sepiol M A and Lucas D M 2016 *Phys. Rev. Lett.* **117** 060504
[17] Gaebler J P *et al* 2016 *Phys. Rev. Lett.* **117** 060505
[18] Wang Y, Um M, Zhang J, An S, Lyu M, Zhang J-N, Duan L-M, Yum D and Kim K 2017 *Nat. Photon.* **11** 646–50
[19] Bermudez A *et al* 2017 *Phys. Rev.* X **7** 041061
[20] García-Ripoll J J, Zoller P and Cirac J I 2003 *Phys. Rev. Lett.* **91** 157901
[21] Garcia O E, Naulin V, Juul Rasmussen J and Nielsen J 2005 *Phys. Plasmas* **12** 062309
[22] Duan L M 2004 *Phys. Rev. Lett.* **93** 100502
[23] Steane A M, Imreh G, Home J P and Leibfried D 2014 *New J. Phys.* **16** 053049
[24] Schäfer V M, Ballance C J, Thirumalai K, Stephenson L J, Ballance T G, Steane A M and Lucas D M 2018 *Nature* **555** 75
[25] Wineland D J, Monroe C, Itano W M, Leibfried D, King B E and Meekhof D M 1998 *J. Res. Natl Inst. Stand. Technol.* **103** 259
[26] Mizrahi J, Senko C, Neyenhuis B, Johnson K G, Campbell W C, Conover C W S and Monroe C 2013 *Phys. Rev. Lett.* **110** 203001
[27] Heinrich D, Guggemos M, Guevara-Bertsch M, Hussain M I, Roos C F and Blatt R 2019 *New J. Phys.* **21** 073017
[28] Holland J H 1973 *SIAM J. Comput.* **2** 88
[29] Holland J H 1975 *Adaptation in Natural and Artificial Systems* (Ann Arbor, MI: University of Michigan Press)
[30] Bentley C D B, Carvalho A R R, Kielpinski D and Hope J J 2013 *New J. Phys.* **15** 043006
[31] Gale E P G, Mehdi Z, Oberg L M, Ratcliffe A K, Haine S A and Hope J J 2020 *Phys. Rev.* A **101** 052328

[32] Hussain M I, Heinrich D, Guevara-Bertsch M, Torrontegui E, García-Ripoll J J, Roos C F and Blatt R 2020 Multi-GHz repetition rate, multi-watt average power, ultraviolet laser pulses for fast trapped-ion entanglement operations (arxiv:2007.03404)
[33] Campbell W C, Mizrahi J, Quraishi Q, Senko C, Hayes D, Hucul D, Matsukevich D N, Maunz P and Monroe C 2010 *Phys. Rev. Lett.* **105** 090502
[34] Malinovsky V S and Krause J L 2001 *Eur. Phys. J.* D **14** 147–55
[35] Wunderlich C, Hannemann T, Körber T, Haeffner H, Roos C, Hänsel W, Blatt R and Schmidt-Kaler F 2007 *J. Mod. Opt.* **54** 1541–9
[36] Heinrich D 2019 Ultrafast coherent excitation of a $^{40}Ca^{+}$ ion *Ph.D Thesis* University of Innsbruck
[37] Bergmann K, Theuer H and Shore B W 1998 *Rev. Mod. Phys.* **70** 1003–25
[38] Vitanov N V, Rangelov A A, Shore B W and Bergmann K 2017 *Rev. Mod. Phys.* **89** 015006
[39] Shapiro E A, Milner V, Menzel-Jones C and Shapiro M 2007 *Phys. Rev. Lett.* **99** 033002
[40] Sørensen J L, Møller D, Iversen T, Thomsen J B, Jensen F, Staanum P, Voigt D and Drewsen M 2006 *New J. Phys.* **8** 261
[41] Møller D, Sørensen J L, Thomsen J B and Drewsen M 2007 *Phys. Rev.* A **76** 062321
[42] Timoney N, Baumgart I, Johanning M, Varón A F, Plenio M B, Retzker A and Wunderlich C 2011 *Nature* **476** 185–8
[43] Palao J P and Kosloff R 2002 *Phys. Rev. Lett.* **89** 188301
[44] Romero-Isart O and García-Ripoll J J 2007 *Phys. Rev.* A **76** 059904
[45] Doria P, Calarco T and Montangero S 2011 *Phys. Rev. Lett.* **106** 190501
[46] Mehdi Z, Ratcliffe A K and Hope J J 2020 Low-requirement fast gates enable quantum computation in long ion chains (arXiv: 2004.04372)
[47] Mehdi Z, Ratcliffe A K and Hope J J 2020 Scalable quantum computation with fast gates in two-dimensional microtrap arrays of trapped ions (arXiv:2005.00367)
[48] Figgatt C, Ostrander A, Linke N M, Landsman K A, Zhu D, Maslov D and Monroe C 2019 *Nature* **572** 368–72
[49] Lu Y, Zhang S, Zhang K, Chen W, Shen Y, Zhang J, Zhang J-N and Kim K 2019 *Nature* **572** 363–7
[50] Martinez E A *et al* 2016 *Nature* **534** 516–9
[51] Knill E 2005 *Nature* **434** 39–44